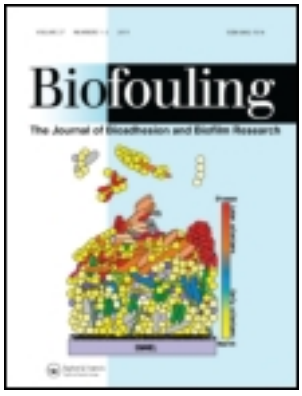

Biofouling: The Journal of Bioadhesion and Biofilm Research

Publication details, including instructions for authors and subscription information:
http://www.tandfonline.com/loi/gbif20

Interfacial morphology and nanomechanics of cement of the barnacle, Amphibalanus reticulatus on metallic and non-metallic substrata

Sangeetha Raman [a] & Ravi Kumar [a]

[a] Department of Metallurgical and Materials Engineering, Indian Institute of Technology - Madras (IIT Madras), Chennai, 600036, India

Version of record first published: 08 Jun 2011.

To cite this article: Sangeetha Raman & Ravi Kumar (2011): Interfacial morphology and nanomechanics of cement of the barnacle, Amphibalanus reticulatus on metallic and non-metallic substrata, Biofouling: The Journal of Bioadhesion and Biofilm Research, 27:6, 569-577

To link to this article: http://dx.doi.org/10.1080/08927014.2011.589027

Biofouling
Vol. 27, No. 6, July 2011, 569–577

Taylor & Francis
Taylor & Francis Group

Interfacial morphology and nanomechanics of cement of the barnacle, *Amphibalanus reticulatus* on metallic and non-metallic substrata

Sangeetha Raman and Ravi Kumar*

Department of Metallurgical and Materials Engineering, Indian Institute of Technology – Madras (IIT Madras), Chennai 600036, India

(*Received 1 February 2011; final version received 13 May 2011*)

The barnacle exhibits a high degree of control over its attachment onto different types of solid surface. The structure and composition of barnacle cement have been reported previously, but mostly for barnacles growing on low surface energy materials. This article focuses on the strategies used by barnacles when they attach to engineering materials such as polymethylmethacrylate (PMMA), titanium (Ti) and stainless steel 316L (SS316L). Adhesion to these substrata is compared in terms of morphological structure, thickness and functional groups of the primary cement, the molting cycle and the nanomechanical properties of the cement. Structural characterization studies using scanning electron microscopy (SEM) and transmission electron microscopy (TEM) in conjunction with nanomechanical characterization and infrared spectroscopy (FTIR) are used to understand the differences in the adhesion of primary barnacle cement to the different substrata. The results provide new insights into understanding the mechanisms at work across the barnacle–substratum interface.

Keywords: barnacle cement; titanium; stainless steel 316L; PMMA; interfacial morphology; nanomechanics

Introduction

Adhesives secreted by marine organisms for permanent adhesion are recognized as some of the most robust in the living world as they are secreted and cured in seawater and anchor the organism firmly during its entire lifetime. The adhesion of mussels, barnacles and tubeworms have provided a challenge for many scientists and a number of publications have examined the morphological structure and chemical composition of the secreted adhesives (Crisp et al. 1985; Stewart et al. 2004; Sun et al. 2004; Lee et al. 2006; Kamino 2010a).

The morphological structure of barnacle cement has been reported to vary between different species. The morphology of the cement also appears to be influenced by the substratum to which the barnacle attaches. Wiegemann and Watermann (2003) reported the presence of a loosely matted, net-like structure for cement of *Balanus improvisus* attached to polydimethylsiloxane (PDMS). On a metallic surface such as aluminum foil, it was reported that the liquid adhesive appeared as globules, which fused to form a thick dense morphology. These reports are based on imaging the cement using scanning electron microscopy (SEM) after dehydration and CO_2 drying. However, Berglin and Gatenholm (2003) reported a totally different morphology for the same species on PDMS. A continuous film-like appearance with a few fused granules was observed for the cement on the barnacle base-plate on PDMS while completely granular morphology was observed for cement remnants on polymethylmethacrylate (PMMA) surface when imaged using atomic force microscopy (AFM). Sullan et al. (2009) found a mixture of globular, mesh-like and rod-like features for the secondary cement of *Amphibalanus amphitrite* reattached to aluminum foil when observed under SEM and AFM. In the latter paper, primary cement was referred to the natural cement secreted during the growth of the adult barnacle while secondary cement was the cement secreted during the process of reattachment after a barnacle has been artificially detached from a surface (Kamino 2010b). Dickinson et al. (2009) reported that AFM revealed a fibrous structure for both the primary cement of the barnacle *A. amphitrite* attached on a silicone substratum as well as for the secondary cement cured on a glass slide under ambient conditions. A fibrillar appearance has also been reported for secondary cement on quartz substrata by Barlow et al. (2010). In a previous study on stainless steel 316L (SS361L) substratum, the morphology reported for the primary cement was fibrous with a mesh-like appearance (Sangeetha et al. 2010a). An assessment of all these studies shows that

*Corresponding author. Email: nvrk@iitm.ac.in

ISSN 0892-7014 print/ISSN 1029-2454 online

DOI: 10.1080/08927014.2011.589027
http://www.informaworld.com

the variation in barnacle cement morphology is a function of the species, the substratum for attachment and also whether it is primary or secondary cement. It has been recognized that apart from the changes associated with the cement morphology, base-plate structure can also be modified in response to the surface energy of the material. On low surface energy materials like silicone rubber and PDMS, it is difficult to see the typical concentric ring-like cement structure. Also, the base-plate is often concave when grown on this type of substratum. The thickness of the cement was around 1 mm (Wiegemann and Watermann 2003), but it varied from the center to the periphery. Despite these reports, no attempt has been made to understand the difference in the morphology of the cement as well as base-plate microstructure developed by the barnacle as a function of the substratum material for attachment.

It is important to understand the morphology of the primary cement of the barnacle as it is associated with its growth being responsible for maintaining the barnacle attached to the substratum for the whole of its lifetime. Attachment is so strong on metallic substrata that the force required to detach a barnacle is less than the mechanical strength of the parietal shell, which results in crushing of the shell before it can be detached. Hence, the present work concentrates on the adhesion of primary cement with respect to three engineering materials: two metallic (ferrous and non-ferrous) and a non-metallic substratum. The adhesion of barnacles on metallic surfaces has not been investigated previously. Microstructural differences of the base-plate and interfacial cement thickness with respect to the three surfaces is also investigated here. Titanium (Ti) was chosen as it is resistant to marine corrosion and barnacles exhibit strong attachment to Ti substrata. SS316L was chosen as it exhibits corrosion resistance to seawater even though it is susceptible to localized corrosion. PMMA was used to compare differences in adhesion with the metallic surfaces. Structural characterization techniques were used in conjunction with nanoindentation measurements to understand the mechanisms at work within the barnacle–substratum interface.

Materials and methods

Contact angle measurement

Contact angles of surfaces of PMMA, Ti and SS316L prior to deployment were measured by the sessile drop method using an Easy Drop Contact Angle Measuring System (Krüss, Germany) with MilliQ water of surface tension 72.8 mN m^{-1}. The substrata were wiped with ethanol prior to the measurement. The data reported here are an average of a minimum of 10 measurements on each substratum surface.

Barnacles and cement characterization

Amphibalanus reticulatus attached to PMMA, Ti and SS316L substrata were collected from the marine waters of the Bay of Bengal (Ennore Port, Chennai). The tissues were removed and the shells were cleaned gently and subsequently allowed to dry in air. The parietal shells were removed from some of the barnacles as only the basal regions attached to the respective substrata were considered in the present study. Barnacle cement that attached the animal to the substratum is seen as an imprint below the base-plate and this imprint is characteristic of the primary cement secreted during growth. The cement, as well as the base-plate free of the cement (after wiping with acetone), was investigated for the three substrata.

The microstructure of the cement and base-plate of barnacles on each substratum was imaged using FEI Quanta 200 (USA) SEM fitted with lithium doped silicon energy dispersive X-ray spectrometer (EDS) (AMETEK Process and Analytical Instruments). The specimens were coated with 6 nm thick Au/Pd prior to SEM examination. Cross-sections were prepared to study the interface by SEM. The substratum underneath the barnacles after wiping away the cement was also imaged to see whether the morphology of the three substrata had been affected.

For transmission electron microscopy (TEM), the dried cement was gently scraped from the substratum using a blade and transferred immediately to a copper grid. This was then observed with a PHILIPS CM20 TEM under bright field imaging condition. The diffraction pattern was collected subsequently for bright field images.

The barnacle cement was scraped from the substrata and pressed into separate pellets with spectroscopically pure KBr. The functional groups of the compounds present in the cement were collected by Fourier transform infrared spectroscopy (FTIR) using a Perkin Elmer (Spectrum, USA) spectrometer in the frequency range of 4000–400 cm^{-1} at a resolution of 4 cm^{-1}.

Measurement of cement hardness and modulus

The hardness and the elastic modulus of the cement were measured using a nanomechanical testing system, TI 950 Triboindenter, Hysitron Inc (USA). The load–displacement curves were plotted using a three-sided pyramidal diamond Berkovich tip with a force resolution of about 50 nN and displacement of about 0.1 nm. The curves were analyzed by the Oliver–Pharr method

(Oliver and Pharr 1992) and the reduced modulus values obtained were converted into Young's modulus, E_{sp}, using the equation:

$$\frac{1}{E_r} = \frac{(1 - v_{sp}{}^2)}{E_{sp}} + \frac{(1 - v_i{}^2)}{E_i}$$

where E_r is the reduced modulus obtained by analyzing the load–displacement curve, v_{sp} is the Poisson's ratio of the specimen (v_{sp} is taken here as 0.3) and E_i and v_i are the Young's modulus and Poisson's ratio of the diamond indenter (1141 GPa and 0.007 respectively). The indentations were carried out on different regions of two or more imprints on each substratum to ensure that the values were representative.

Results

The contact angle measurements of the three substrata are shown in Table 1. The detachment of a barnacle base-plate from the substratum results in non-uniform distribution of cement (Figure 1a). Part of the cement remains on the substratum; the rest is associated with the base-plate. In order to determine the interfacial structure, systematic SEM observations were carried out on the detached regions of both the substratum and the base-plate (fractured zones of cement; see Figure 1b). Since the samples were dry and also had a conductive coating on their surfaces, no distortion of the true microstructure was observed. The SEM micrographs of the dried cement imprint left on PMMA, Ti and SS316L substrata after removing the barnacles are depicted in Figure 2a–c. The cement has sponge-like structure on PMMA (Figure 2a) in contrast to a more porous, broad-stranded monolayer of cement on the surface of Ti with strands of size in the range of 2 μm (Figure 2b). The fibrous cement remnant on the SS316L surface had interacted with the grain boundaries and preferentially etched them as seen in Figure 2c. The broad strands on Ti have fibre-like features over them (Figure 2b) indicating there were connections present above them before detachment. Lower magnification images of the cement on the three substratum materials are provided in the Supplementary information [Supplementary material is available *via* a multimedia link on the online article webpage] (Figure S1).

The cement attached to the base-plates of barnacles grown on PMMA and Ti is shown in Figure 3a and b. The cement remaining on the base-plate from PMMA (Figure 3a) shows the same morphology as in Figure 2a, which indicates the absence of fibrous structures. The cement strands are 80 to 100 nm thick in the case of Ti and are uniformly linked and appear foam-like (Figure 3b). This suggests that there is a variation in

Table 1. Contact angle measurement of the substratum materials.

Substratum	Average contact angle (°)
Titanium	66.1 ± 2.9
Stainless steel 316L	65.8 ± 2.8
PMMA	79.7 ± 1.9

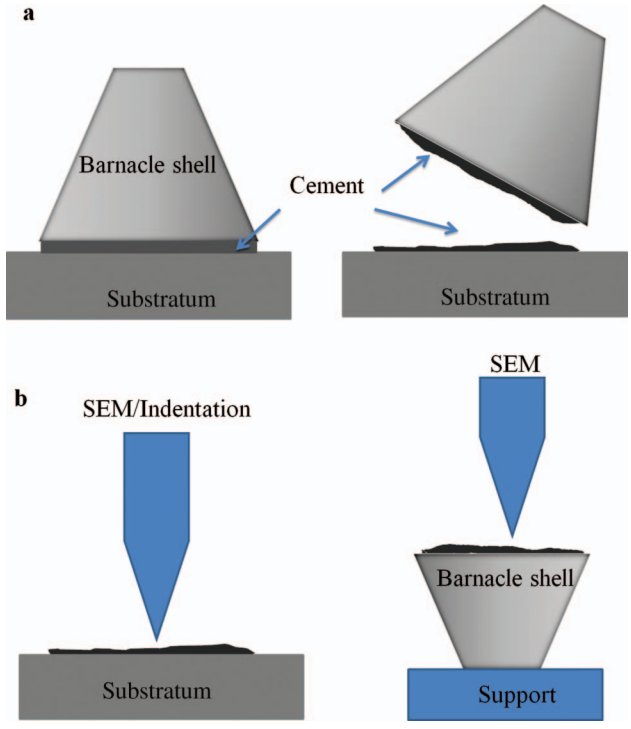

Figure 1. (a) Schematic of an adult barnacle shell attached to a substratum by cement showing that detachment always results in non-uniform distribution of cement on the base-plate as well as the substratum; (b) schematic representing the locations of SEM and nanoindentation measurements.

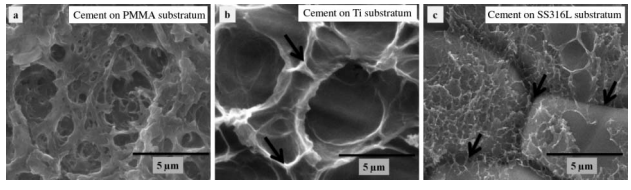

Figure 2. (a) Thick dense sponge-like cement left on PMMA substratum; (b) broad-stranded layer of cement on Ti. The broad strands have fine fibrous structures over them indicating the pre-existing connections; (c) SS316L substratum viewed through the translucent barnacle cement where the grain boundaries (marked by arrows) are seen etched by the barnacle cement.

cement structure between the base-plate and the substratum in case of Ti, whereas, in the case of PMMA, there is no such gradient of microstructure. The gradient of cement morphology on Ti is shown in the Supplementary information [Supplementary material is available *via* a multimedia link on the online article webpage] (Figure S2). The broad cement strands attached to the metal surface have tiny strands emerging from them which connect to the base-plate (Supplementary information [Supplementary material is available *via* a multimedia link on the online article webpage] Figure S2b and c). The broad strands are however connected to the substratum through a thin sheet of cement which can be observed in Supplementary information [Supplementary material is available *via* a multimedia link on the online article webpage] Figure S2a. Figure 3c corresponds to the cement structure remnant on SS316L, where, it can be observed that the fibrous structures emerge from a thin sheet-like layer of cement. This type of sheet-like cement structure at the immediate interface is seen for all the substratum materials. Also, such sheets are visible as the observations progress towards the vicinity of the base-plate, which is reported earlier (Sangeetha et al. 2010a). Although the interface could not be clearly imaged for SS316L due to interaction of the cement with the substratum, fibrous strands of similar dimensions were observed at all instances on different regions of base-plate and the substratum.

The bright field TEM images of the scraped cement, which are depicted in Figure 4 for the three substrata, complement the SEM images. The diffraction patterns indicating an amorphous halo are provided as inserts for the cement structures. The micrographs also indicate a thick dense structure for PMMA (Figure 4a) and a fibrous structure for both Ti (Figure 4b) and SS316L (Figure 4c) substrata.

The concentric rings on the base-plate of the barnacles detached from all three substrata are depicted in Figure 5. The separation gap between adjacent rings is measured to be 75 μm for barnacles on PMMA (Figure 5a) while those from Ti and SS316L (Figure 5b and c) have a similar gap of approximately 350 μm between adjacent rings.

A comparative study of the cement thickness on each substratum was performed using SEM (Figure 6). The interfacial thickness of the cement binding the base-plate and the substratum is about 30 μm for PMMA (Figure 6a), while the thickness observed for Ti (Figure 6b) and SS316L (Figure 6c) is in between 2 to 3 μm.

The substrata after removal of the cement also appear different (Figure 7). PMMA and Ti appear to have damage only at the center of the barnacle (ie the center of the concentric rings). The rest of the substratum appears unaffected away from the center towards the periphery. However, the area of damage at the center is different for the two substrata. PMMA has a larger damaged area enveloping $\sim$4.25 mm (Figure 7a) while that of Ti is $\sim$150 μm (Figure 7b). Although the area of damage to the substratum surface by the cement is around 4.5 mm for SS316L, the rest of the barnacle-attached region also suffers from selective etching of the grain boundaries (Figure 7c).

The FTIR spectrum of dried barnacle cement is indicated in Figure 8. The different peaks are identified for the three substrata and tabulated in Table 2. It is worth noting that in spite of the morphological differences with respect to the substratum, the functional groups are the same in all three cases.

Figure 9a shows a representative image of the cement where indents were made (see Figure 1b). In

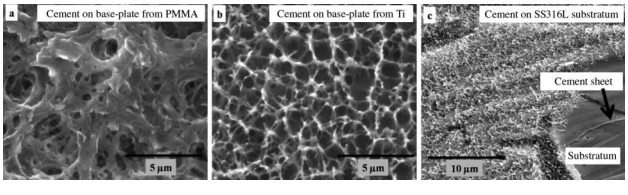

Figure 3. The cement structure towards the base-plate of the barnacle showing the differences in morphology between PMMA (a) and Ti (b); on PMMA, fibres are not visible and cement on Ti has more open space volume; (c) represents the fibrous cement structure on the SS316L substratum and also shows a thin dense sheet of cement from which the fibrous structures emerge.

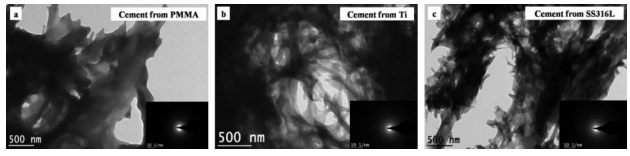

Figure 4. TEM images of barnacle cement. The cement is amorphous irrespective of the attachment surface, though there is a variation in the cement structure. The diffraction pattern of the cement showing amorphous halo is provided as insert in each micrograph.

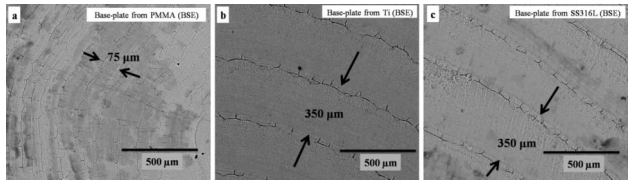

Figure 5. Concentric ring spacing as a measure of the number of molting cycles of the barnacle. Note the ring spacing is large for Ti (b) and SS316L (c), showing fewer molting cycles than when grown on PMMA (a).

order to optimize the load required for deforming the cement, a wide range of loads was applied starting from 50 μN; imaging of the indent was performed simultaneously. It is observed that up to 200 μN of load the material showed complete recovery and the indent impression disappeared in two imaging scans. Above 200 μN, plastic deformation of the material occurred and hence, all the indents were performed with a load of 750 μN so that there was significant plastic deformation without any substratum effects. The load–displacement curves were plotted for a minimum of ten indents. The mean hardness, reduced modulus, elastic modulus and contact depth measured are provided in Table 3. A comparison of two representative load–displacement plots of cements left on PMMA and Ti is made in Figure 9b along with the indent impression images in Figure 9c and d.

Discussion

Strong adhesion requires spreading of an adhesive over the surface. A low contact angle for a surface implies the adhesive will wet the surface better, thus improving the quality of adhesion to that surface. Both the metallic surfaces had similar contact angles and they were lower than the non-metallic substratum. Detachment of barnacles from metallic surfaces is generally more difficult than from non-metallic ones and this may be the reason why few studies have been reported regarding adhesion to metallic substrata. In this study, an attempt was made to understand the adhesion behavior of barnacles on metallic and non-metallic surfaces by comparing the number of molting cycles (based on the number of concentric rings on the base-plate), cement morphology, cement thickness as well as the nanomechanical properties of the cement.

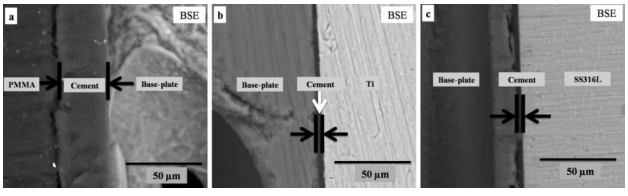

Figure 6. Interfacial thickness of the barnacle cement is related to the number of molting cycles. The thickness of the cement is higher for PMMA (a) compared to that on the metallic surfaces which have same thickness (b and c).

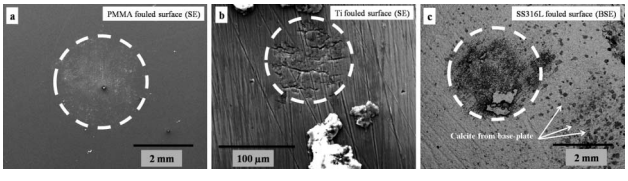

Figure 7. SEM images of substrata after cement was removed by wiping. The interaction of the cement with the surfaces is visible and the area of damage is different in each case.

Microstructure of the barnacle cement

Surfaces when exposed to marine waters adsorb organic material from their surroundings to form a polymeric layer, commonly referred to as the conditioning film. Glycoproteins, humic acids, proteins, amino acids and carbohydrates are identified to be the key components of the conditioning film (Jain and Bhosle 2009). The surface chemistry is altered and the physical parameters such as wettability and roughness

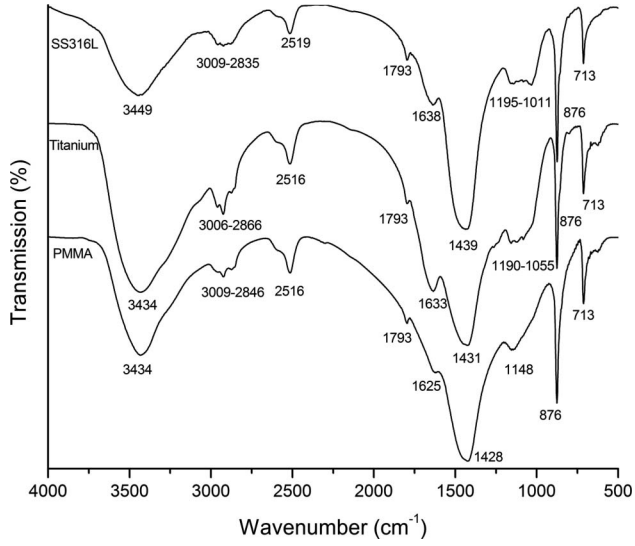

Figure 8. FTIR spectra of cement on the three substrata comparing the relative intensities of the functional groups present.

Table 2. Band assignment for the peaks for the barnacle cement from three different substrata.

PMMA (cm^{-1})	Ti (cm^{-1})	SS316L (cm^{-1})	Band assignment
3434	3434	3449	Water O−H stretching
3009–2846	3006–2866	3009–2835	Aliphatic C−H stretching
2516	2516	2519	S−H stretching
1793	1793	1793	C=O non-conjugate vibration
1625	1633	1638	Amide I
1428	1431	1439	CH_2 bending
1148	1190–1055	1195–1101	C−O stretching
876	876	876	$CaCO_3$
713	713	713	$CaCO_3$

Table 3. Nanomechanical properties of the cement.

Substratum	Hardness (MPa)	Modulus (GPa)		Contact depth (nm)	Barnacle cement interfacial thickness
		E_r	E_{sp}		
PMMA	52.56 ± 12.18	1.32 ± 0.16	1.20 ± 0.16	682.6 ± 42.3	~30 μm
Ti	8.72 ± 1.19	0.47 ± 0.04	0.43 ± 0.04	1802.6 ± 138.6	~3 μm

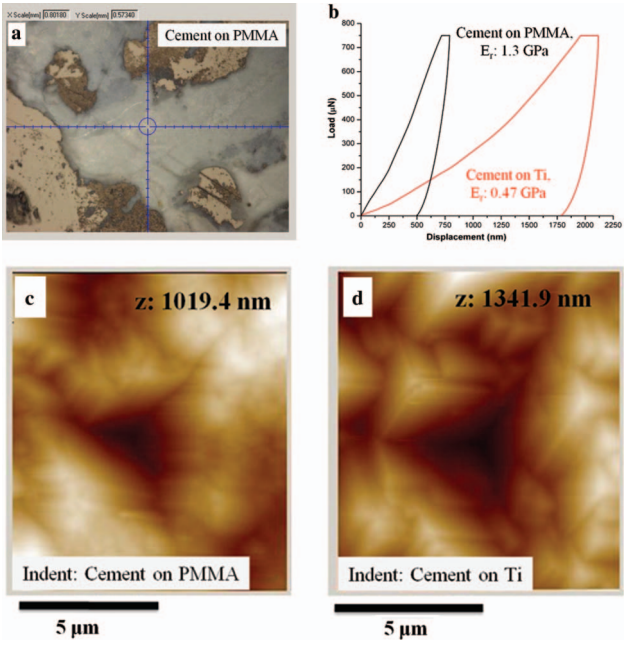

Figure 9. (a) Representative optical image of the position of indentation; (b) load-displacement curves of the cement on PMMA and Ti surfaces; the respective indent impressions on the cement on (c) PMMA and (d) Ti, imaged in height mode using the diamond indenter tip.

are modified due to the presence of the conditioning layer (Bakker et al. 2004; Jain and Bhosle 2009). Bacterial adhesion and colonization to the conditioned surfaces result in the formation of a biofilm favoring the settlement of larvae of the macrofouling invertebrates. However, the adhesive of the macrofoulers during growth penetrates the biofilm and conditioning film to establish direct contact with the original surface for firm adhesion. The wettability of the pristine surfaces of the substrates eventually defines the adhesion behavior of the macrofouling species. This has been found to be true for both mussels and barnacles (Wiegemann 2005; Sangeetha et al. 2010a).

Barnacle cement has been reported to be hydrophilic in nature (Barlow et al. 2009), although the studies of Naldrett and Kaplan (1997) and Kamino et al. (2008) show the presence of hydrophobic components. Metallic surfaces have a higher hydrophilicity due to delocalized electrons and help the barnacle cement to spread over the surface. It was observed that strands developed after the formation of an initial sheet-like cement layer that completely covered the substratum surface mimicking the surface features. This is further proof that the liquid cement wets the surface prior to developing fibrous structures. However, the reasons for the development of different morphology on Ti and SS316L are not known. On the other hand, due to the lower wettability of the surface the cement wets the PMMA surface less readily than the metallic surfaces. This is evident from the morphology itself as hardly any fibrous structure could be located in cement on PMMA (see Figure 2a). The thermal conductivity of the substratum will also help in transferring heat from the cement, thus facilitating faster solidification. The values reported for the thermal conductivity of the three materials are 0.19 W mK^{-1} for PMMA (Assael et al. 2005), 27 W mK^{-1} for Ti (Basu et al. 2010) and 14 W mK^{-1} for SS16L (Kowalski et al. 1999). The lower value of conductivity for PMMA may also explain why the cement solidified on its surface had no fibrous morphology. The differences in cement morphologies on Ti and SS316L can also be attributed to the difference in thermal conductivity, which plays a major role in defining the solidification pattern of any liquid adhesive.

The concentric rings present on the base-plate are an indicative of the molting cycles of the barnacles associated with their growth (Saroyan et al. 1970; Lindner 1984; Khandeparker and Anil 2007; Sangeetha et al. 2010b), cement secretion taking place between adjacent molting cycles. Secretion occurs outside the base-plate through the uniformly shaped cracks (cement duct ends) that are visible over the concentric rings. A greater number of concentric rings, indicates a greater number of molting cycles. The base-plates on PMMA had a greater number of concentric rings than those on either the Ti or SS316L substrata, which means that the barnacles secreted more cement on the PMMA than on the metals. This can be directly linked to the thickness of the cement on each substratum. The cross-section studies revealed that only a thin layer (~3 μm) of cement was needed for attachment onto the metallic substrata while PMMA substrata required nearly ten times more cement for firm adhesion. This indicates a common trend in the

attachment behavior of barnacles on metallic substrata, adhesion being comparatively easier to these high energy surfaces. Furthermore, barnacles have to undergo several molting cycles on order to secrete the amount of cement needed for firm adhesion to the polymeric surface. Thus the molting process appears to be influenced by the nature of the attachment surface. The increase in cement thickness can also be one of the reasons for the spongy cement structure on PMMA as it takes longer to cure thereby failing to form fibres.

Interaction between the barnacle and the surface was investigated by completely removing the cement from the substratum. When the central region of barnacle attachment was observed, localized surface modification was visible. This region can be considered as the site of initial attachment of the cyprid prior to metamorphosis. Although the same process occurred on all the substrata, the chemical interaction between cement and the SS316L surface was more prominent, resulting in the corrosion of the substratum. This interaction has been reported earlier and a mechanism was proposed to explain the etching phenomenon (Sangeetha et al. 2010a). Selective etching of the grain boundaries by the barnacle cement is always observed, which is considered as a precursor to localized corrosion beneath the barnacle base. This kind of interaction was not observed for Ti. It is known that Ti has a passive layer of oxide over its surface, which would prevent direct contact of the cement with the metal thus protecting it from any corrosion. This is true for the SS316L surface also, however, it appears that the passive chromium oxide is removed by some unknown interaction of the cement initiating corrosion process. In case of PMMA, the hydrophobic nature of the surface weakens the attachment of the cement providing it with few sites to induce degradation.

Functional groups in barnacle cement

Infrared spectral analysis of the barnacle cement demonstrated consistent peak positions for the different base materials. The peak position between 3200 to 3500 cm^{-1} indicates the presence of water in the dried primary cement. The intensity of the peak was higher for Ti suggesting a higher water content. The remaining peaks correspond to the typical protein band positions reported earlier (Barth 2007; Barlow et al. 2009). The band position between 2515 to 2590 cm^{-1} suggests the presence of the S—H bearing amino acid cystine that contributes to forming disulfide bonds (Barth 2007). The presence of cystine was reported earlier by Naldrett and Kaplan (1997) and Kamino et al. (2000) for *Megabalanus rosa* and *Balanus crenatus*, respectively and they showed that the disulfide bonds have a major role in making the barnacle cement insoluble. The presence of disulfide bonds, however, was not observed in the cement collected from *Balanus crenatus* adhesive protein (Wiegemann et al. 2006). Reports on the primary cement interfaces of *A. amphitrite* also do not comment on the presence of any peaks over this region. The peak position at $\sim$1635 cm^{-1} can be assigned as Amide I band for proteins. It has been reported that proteins with fibrous structures contain β-sheets and Barlow et al. (2010) reported that the fibrous structures in the barnacle cement were amyloid fibres that have functional roles. However, it is not certain if the cement of *A. reticulatus* has a similar secondary structure to that of *A. amphitrite*. In addition to the peaks corresponding to proteins, calcium carbonate appears as sharp peaks, suggesting the presence of crystalline calcite in the cement. The calcite probably arises from traces of base-plate that were retained in the cement during mechanical detachment of the shell from the substratum. However, the TEM diffraction pattern does not show any crystalline components, suggesting that the cement is purely amorphous, although EDS of the cement fibres show traces of calcium. It is possible that the cement has calcium incorporated in it to enhance its mechanical properties. It has been reported that the curing of barnacle cement involves glutamyl-lysine cross-linking *via* the action of transglutaminase, a process similar to blood clotting in both vertebrates and invertebrates (Dickinson et al. 2009). However, the above hypothesis has been recently disproved by Kamino (2010b) and the details of the molecular mechanisms involved in the curing process of barnacle cement still remains as an open question which requires further attention in order to understand how the cement solidifies in seawater.

Mechanical properties of the barnacle cement

Calcareous marine foulers employ different techniques for anchoring themselves to hard surfaces. Mussels secrete byssal threads of a collagen core protected by a hard cuticle that incorporates metal ions (Inoue et al. 1995; Zhao and Waite 2005, 2006). The nanomechanical properties of mussel byssus are known for several species. The modulus value for the cuticle of both *Mytilus californianus* and *Mytilus galloprovincialis* (Andersen et al. 2007; Andersen and Waite 2008; Andersen et al. 2009) has been determined as 1.7 GPa, with hardness $\sim$ 100 MPa. The inner fibrous collagen core of both species has modulus and hardness values of 0.4 GPa and 20 MPa, respectively. For *Perna canaliculus* (Andersen et al. 2007) values for modulus and hardness are 0.37 GPa and 19.4 MPa, respectively,

for the collagen and 2.3 GPa and 133 MPa, respectively for the cuticle. The layered adhesive secreted by the tubeworm *Hydroides dianthus* is also proteinaceous in nature. Due to the dispersion of Mg-calcite and aragonite crystals, the adhesive has a superior stiffness of $\sim$3 GPa measured by AFM (Tanur et al. 2010). The only literature available on the mechanical properties of barnacle cement was reported for the species *A. amphitrite* (Sullan et al. 2009), where AFM indentation was used to determine the elastic modulus by pulling out single molecules of cement. The modulus ranged from 0.0002–0.09 GPa for the rod-like structures, unstructured aggregates and the fibrous matrix found in the cement.

In the work presented in this article, nanoindentation at lower loads suggests that the barnacle cement is viscoelastic in nature. However, at higher loads, the mechanical properties of the cement also show a profound variation in hardness and modulus values with respect to the adhering substratum. Since the adhesion strength of the barnacles on metallic surfaces is greater than non-metallic substrata, it was expected that the mechanical properties would be superior for the cement on Ti substratum. However, nanoindentation studies revealed that the nanomechanical properties are superior for the cement on PMMA. One possible explanation can be made based on the morphological differences of cement across the interface on both substratum materials, especially with respect to open volume. Based on positron annihilation spectroscopy analysis, it has been reported that secondary cement of *Balanus crenatus* has a pore size of up to 0.5 nm diameter (Rätzke et al. 2010). This shows that an open volume up to sub-nanometric scale exists, which will exert control over the nanomechanical properties. As the indenter tip progresses through the cement on Ti, the strands are ruptured as they are thin at the top region. Due to more open volume, the tiny strands collapse easily, resulting in a lower modulus value. However, the indenter does not hit the substratum as the load was optimized not to reach the surface. On PMMA, the cement is a dense fused structure and the open volume is also considerably less preventing the tip going deeper, which results in comparatively higher stiffness. This is also reflected in the lower contact depth observed while indenting the cement on PMMA. To answer the question why the interface on Ti is strong requires analysis at the macroscale. In effect, the load is not localized to a few strands, but distributed all over the viscoelastic interface, which prevents the fracture of individual strands on application of load. In the case of PMMA, detachment is easier because there are no fibrous connections across the interface to be ruptured prior to dislodgement.

Summary

Analysis of the attachment interfaces of barnacles growing on three different substrata showed that the cement was amorphous and carried the same functional groups. However, the morphology of the cement differed between substrata. A fibrous morphology developed from a thin sheet of cement was commonly observed for the metallic substrata, whereas a sponge-like microstructure with pores of different sizes and morphology was observed for PMMA. The barnacle was attached by only a 3 μm thick layer of cement on the metallic surfaces, but the layer was around 30 μm on PMMA. The number of concentric rings per unit area on the base-plate reflected the quantity of cement secreted on the different substrata. Localized interaction of the cement was observed for all the three substrata, especially for SS316L. Nanoindentation studies showed that the cement was viscoelastic in nature at lower loads and was influenced by the open volume present, which in turn was substratum dependent. The results presented provide a comprehensive understanding of the fundamentals of barnacle adhesion to simple engineering materials.

Acknowledgements

The contact angle measurements were carried out at the Department of Biotechnology, IIT Madras, which is gratefully acknowledged. The authors thank Ms D. Kanchanamala, Senior Technical Assistant, IIT Madras, for the TEM imaging. The authors also thank the Sophisticated Analytical Instruments Facility (SAIF), IIT Madras, for carrying out the FTIR measurements.

References

Andersen NH, Waite JH. 2008. Mussel-designed protective coatings for compliant substrates. J Dent Res 87:701–709.

Andersen NH, Zhao H, Waite JH. 2009. Stiff coatings on compliant biofibers: the cuticle of *Mytilus californianus* byssal threads. Biochemistry 48:2752–2759.

Andersen NH, Fantner GE, Hohlbauch S, Waite JH, Zok FW. 2007. Protective coatings on extensible biofibres. Nat Mater 6:669–672.

Assael MJ, Botsios S, Gialou K, Metaxa IN. 2005. Thermal conductivity of polymethyl methacrylate (PMMA) and borosilicate crown glass BK7. Int J Thermophys 26:1595–1605.

Bakker DP, Busscher HJ, van Zanten J, de Vries J, Klijnstra JW, van der Mei HC. 2004. Multiple linear regression analysis of bacterial deposition to polyurethane coatings after conditioning film formation in the marine environment. Microbiology 150:1779–1784.

Barlow DE, Dickinson GH, Orihuela B, Rittschof D, Wahl KJ. 2009. *In situ* ATR-FTIR characterization of primary cement interfaces of the barnacle *Balanus amphitrite*. Biofouling 25:359–366.

Barlow DE, Dickinson GH, Orihuela B, Kulp JL, Rittschof D, Wahl KJ. 2010. Characterization of the adhesive plaque of the barnacle *Balanus amphitrite*: amyloid-like nanofibrils are a major component. Langmuir 26:6549–6556.

Barth A. 2007. Infrared spectroscopy of proteins. Biochim Biophys Acta Bioenerg 1767:1073–1101.

Basu B, Mukhopadhyay A, Mishra A, Sarkar J. 2010. Does thermal conductivity play a role in sliding wear of metals in cryogenic environment? J Tribol 132. 041604-1–041604-5.

Berglin M, Gatenholm P. 2003. The barnacle adhesive plaque: morphological and chemical differences as a response to substrate properties. Colloids Surf B 28:107–117.

Crisp DJ, Walker G, Young GA, Yule AB. 1985. Adhesion and substrate choice in mussels and barnacles. J Colloid Interface Sci 104:40–50.

Dickinson GH, Vega IE, Wahl KJ, Orihuela B, Beyley V, Rodriguez EN, Everett RK, Bonaventura J, Rittschof D. 2009. Barnacle cement: a polymerization model based on evolutionary concepts. J Exp Biol 212:3499–3510.

Inoue K, Waite JH, Matsuoka M, Odo S, Harayama S. 1995. Interspecific variations in adhesive protein sequences of *Mytilus edulis, M. galloprovincialis* and *M. trossulus*. Biol Bull 189:370–375.

Jain A, Bhosle NB. 2009. Biochemical composition of the marine conditioning film: implications for bacterial adhesion. Biofouling 25:13–19.

Kamino K. 2008. Underwater adhesive of marine organisms as the vital link between biological science and material science. Mar Biotech 10:111–121.

Kamino K. 2010a. Molecular design of barnacle cement in comparison with those of mussel and tubeworm. J Adhesion 86:96–110.

Kamino K. 2010b. Absence of cross-linking *via* transglutaminase in barnacle cement and redefinition of the cement. Biofouling 26:755–760.

Kamino K, Inoue K, Maruyama T, Takamatsu N, Harayama S, Shizuri Y. 2000. Barnacle cement proteins: importance of disulfide bonds in their insolubility. J Biol Chem 275:27360–27365.

Khandeparker L, Anil AC. 2007. Underwater adhesion: the barnacle way. Int J Adhes Adhes 27:165–172.

Kowalski L, Duszczyk J, Katgerman L. 1999. Thermal conductivity of metal powder-polymer feedstock for powder injection moulding. J Mater Sci 34:1–5.

Lee H, Scherer NF, Messersmith PB. 2006. Single-molecule mechanics of mussel adhesion. Proc Natl Acad Sci USA 103:12999–13003.

Lindner E. 1984. The attachment of macrofouling invertebrates. In: Costlow JD, Tipper RC, editors. Marine biodeterioration: an interdisciplinary study. Annapolis (MD): US Naval Institute. p. 183–201.

Naldrett MJ, Kaplan DL. 1997. Characterization of barnacle (*Balanus eburneus* and *B. crenatus*) adhesive proteins. Mar Biol 127:629–635.

Oliver WC, Pharr GM. 1992. An improved technique for determining hardness and elastic modulus using load and displacement sensing indentation experiments. J Mater Res 7:1564–1583.

Rätzke K, Wiegemann M, Shaikh MQ, Harms S, Adelung R, Egger W, Sperr P. 2010. Open volume in bioadhesive detected by positron annihilation lifetime spectroscopy. Acta Biomater 6:2690–2694.

Sangeetha R, Kumar R, Doble M, Venkatesan R. 2010a. Barnacle cement: an etchant for stainless steel 316L? Colloids Surf B 79:524–530.

Sangeetha R, Kumar R, Venkatesan R, Doble M, Vedaprakash L, Kruparatnam, Lakshmi K, Dineshram. 2010b. Understanding the structure of the adhesive plaque of *Amphibalanus reticulatus*. Mater Sci Eng C 30:112–119.

Saroyan R, Lindner E, Dooley CA. 1970. Repair and reattachment in Balanidae as related to their cementing mechanism. Biol Bull 139:333–350.

Stewart RJ, Weaver JC, Morse DE, Waite HJ. 2004. The tube cement of *Phragmatopoma californica*: a solid foam. J Exp Biol 207:4727–4734.

Sullan RMA, Gunari N, Tanur AE, Chan Y, Dickinson GH, Orihuela B, Rittschof D, Walker GC. 2009. Nanoscale structures and mechanics of barnacle cement. Biofouling 25:263–275.

Sun Y, Guo S, Walker GC, Kavanagh CJ, Swain GW. 2004. Surface elastic modulus of barnacle adhesive and release characteristics from silicone surfaces. Biofouling 20:279–289.

Tanur AE, Gunari N, Sullan RMA, Kavanagh CJ, Walker GC. 2010. Insights into the composition, morphology, and formation of the calcareous shell of the serpulid *Hydroides dianthus*. J Struct Biol 169:145–160.

Wiegemann M. 2005. Adhesion in blue mussels (*Mytilus edulis*) and barnacles (genus *Balanus*): mechanisms and technical applications. Aquat Sci 67:166–176.

Wiegemann M, Watermann B. 2003. Peculiarities of barnacle adhesive cured on non-stick surfaces. J Adhes Sci Technol 17:1957–1977.

Wiegemann M, Kowalik T, Hartwig A. 2006. Noncovalent bonds are key mechanisms for the cohesion of barnacle (*Balanus crenatus*) adhesive proteins. Mar Biol 149:241–246.

Zhao H, Waite JH. 2005. Coating proteins: structure and cross-linking in fp-1 from the green shell mussel *Perna canaliculus*. Biochemistry 44:15915–15923.

Zhao H, Waite JH. 2006. Linking adhesive and structural proteins in the attachment plaque of *Mytilus californianus*. J Biol Chem 281:26150–26158.